Pulkkinen, Mika; Halonen, Kari

Outlooks on Transmitter Energy Efficiency and FOM and a 189.7-dBJ/bit ULP DPPM Transmitter

Published in:
IEEE Transactions on Circuits and Systems I: Regular Papers

DOI:
10.1109/TCSI.2023.3238312

Published: 01/04/2023

Document Version
Publisher's PDF, also known as Version of record

Outlooks on Transmitter Energy Efficiency and FOM and a −189.7-dBJ/bit ULP DPPM Transmitter

Mika Pulkkinen, *Member, IEEE*, and Kari Halonen, *Member, IEEE*

***Abstract*— In this paper, we compare in a new way the energy efficiencies of modulations that have been popular in ultra-low power (ULP) transmitters. The comparison considers how the choice of modulation affects the combined energy consumed per bit (EPB) by the carrier synthesizer and power amplifier (PA). The comparison includes on-off keying (OOK), binary phase-shift keying (BPSK), binary frequency-shift keying (BFSK), pulse-position modulation (PPM) and differential PPM (DPPM). The results suggest that using OOK, BPSK or BFSK can consume tens to hundreds of percents more energy per bit compared to PPM and DPPM. Furthermore, a new energy efficiency figure of merit (FOM) is derived for transmitters. It accounts for consumed power, output power, data rate, signal bandwidth and signal-to-noise ratio required by the utilized modulation. The FOM can be applied to various types of transmitters with numerous modulations. We also present a sub-100 μW DPPM transmitter (TX) and a 3.2-μW 2-axis gesture sensor interface, implemented in 0.18 μm CMOS. The TX operates in the 433-MHz band, uses pulse shaping for improved spectrum and achieves a FOM of −189.7 dBJ/bit. The estimated uplink range is up to 1 kilometer.**

***Index Terms*— Radio transmitter, energy efficiency, figure of merit, differential pulse-position modulation, on-off keying, binary phase-shift keying, binary frequency-shift keying.**

I. Introduction

THE number of wireless devices continues to grow at a rapid pace. Wireless devices are powered by batteries, rechargeable batteries or energy harvesters, all of which are only able to provide a limited amount of power and energy [1], [2]. To reduce the frequency of power outages due to either a dead battery or insufficient harvested energy, it is desirable to minimize the power and energy consumption of all electronic circuits within the device. Radios can consume a significant proportion of the total power in a wireless device and particularly in a sensor node [2]. Designers and researchers have therefore innovated numerous ways to create transmitters (TXs) and receivers (RXs) that achieve sub-mW power consumption. Sub-mW transmitters have generally used binary modulations such as on-off keying (OOK), binary phase-shift keying (BPSK) and binary frequency-shift keying (BFSK) [2], [3], [4], [5], [6], [7], [8], [9], [10], [11], [12], [13]. These simple modulation schemes enable the use of low-complexity low-power transmitter architectures. Therefore, some of the transmitters in [2], [3], [4], [5], [6], [7], [8], [9], [10], [11], [12], and [13] have achieved power consumptions even lower than 100 μW and consumed down to 16.5 pJ of energy per transmitted bit.

In [1], we discussed the benefits of M-ary modulations. These have the potential to achieve higher transmitter energy efficiency compared to binary modulations due to the reduced active time per bit of high-power transmitter circuits. We proposed the use of M-ary differential pulse-position modulation (DPPM) for ultra-low power (ULP) transmitters. It was calculated that the use of 64-DPPM can reduce the consumed energy per bit (EPB) by up to 67% compared to OOK without deteriorating error performance. The presented 64-DPPM transmitter consumed 67 nW and 14 pJ/bit transmitting data in packet-mode at data rate $R_b = 4.8$ kbps. Despite the low EPB, a 30-meter uplink range was achieved in measurements. Thus, [1] showed the potential of M-ary DPPM regarding ULP transmitters and its energy efficiency compared to OOK.

In this article, we continue the work of [1] and compare DPPM not only with OOK, but additionally with BPSK, BFSK and pulse-position modulation (PPM). The majority of power in ULP transmitters is consumed by the carrier synthesizer and power amplifier (PA) [3]. Thus, we shall analyze how the choice of modulation affects the combined energy consumption of these blocks. The results suggest that if the transmitter power consumption is not dominated by the PA, the energy efficiency of a modulation is significantly impacted by the active ratio and active time per bit of the modulation. This favors the use of M-ary modulations. Furthermore, the results suggest that OOK, BPSK and BFSK consume tens to hundreds of percents greater energy per bit compared to M-ary PPM and DPPM for the same error performance.

To evaluate the energy efficiencies of radio transmitters, we derive a new figure of merit (FOM) for transmitter energy efficiency. Prior energy-related FOMs such as EPB [2], EPB per output power [2] or EPB per power efficiency [7] have

Manuscript received 27 July 2022; revised 3 November 2022 and 12 December 2022; accepted 3 January 2023. Date of publication 27 January 2023; date of current version 31 March 2023. This work was supported in part by the Naked Approach (40336/14, 3246/31/2014) and Towards Digital Paradise (2727/31/2016) projects granted by Business Finland and in part by the EffiNano project (1/2014) granted by the Aalto University School of Electrical Engineering. The work of Mika Pulkkinen was supported in part by the Aalto ELEC Doctoral School and in part by the Nokia Foundation. This article was recommended by Associate Editor S. Liu. *(Corresponding author: Mika Pulkkinen.)*

Mika Pulkkinen is with CoreHW Oy, 00180 Helsinki, Finland (e-mail: mika.pulkkinen@aalto.fi).

Kari Halonen is with the Department of Electronics and Nanoengineering, Aalto University School of Electrical Engineering, 02150 Espoo, Finland (e-mail: kari.halonen@aalto.fi).

Color versions of one or more figures in this article are available at https://doi.org/10.1109/TCSI.2023.3238312.

Digital Object Identifier 10.1109/TCSI.2023.3238312

neglected signal bandwidth (BW) and signal-to-noise ratio (SNR). However, SNR is highly related to bit error probability and achievable uplink range [14], [15], [16], [17] and should be accounted for. The mentioned FOMs are also affected by data rate in an irrational manner. The presented new FOM accounts for EPB, maximum SNR achievable with the output signal and the SNR requirement of the utilized modulation. Compared to earlier FOMs, it enables a fairer energy efficiency comparison between transmitters that differ in terms of modulation, data rate, consumed power and output power.

In addition to the theoretical part, we present a novel OOK, PPM and DPPM compatible transmitter and a 3.2-μW 2-axis gesture sensor interface, implemented in 0.18 μm CMOS. The peak output power of the transmitter is −2.1 dBm. It, nevertheless, consumes only 1.56 μW of power when 48-bit 64-DPPM encoded data packets are transmitted at the sensor output sample rate, i.e. 47.2 packets per second (approx. 2.27 kpbs). Pulse shaping is used to reduce occupied bandwidth (OBW) and power in the spectrum side lobes. The transmitter achieves a state-of-the-art energy efficiency FOM of −189.7 dBJ/bit. The estimated uplink range is up to 1 km.

The structure of this paper is as follows. In Sections II and III, we revise the basics of OOK, BPSK, BFSK, PPM and DPPM. Regarding the energy efficiency analysis, we are mainly interested in their error performances, null-to-null bandwidths, noise bandwidths and active ratios. The energy efficiencies of these modulations are compared in Section IV and the energy efficiency FOM is derived in Section V. Section VI presents the implemented transmitter and the gesture sensor interface. Section VII presents the measurement results and an energy efficiency comparison with other ULP transmitters.

II. OOK, BPSK AND BFSK

OOK, BPSK and BFSK are binary modulations that encode one bit per symbol by toggling the amplitude, phase or frequency of the carrier wave, respectively, to one of two values that represent bits 1 and 0 [14], [15], [16], [17]. The modulator is clocked at a baseband clock frequency $f_{BB} = 1/T_{BB}$, one 1-bit symbol is transmitted in duration T_{BB}, and the data rate is $R_b = f_{BB}$. When the error probabilities of these and other modulations are discussed in this work, the term $\gamma = E/N_0$ refers to signal-to-noise ratio (SNR) and $\gamma_b = E_b/N_0$ refers to the SNR per bit [14], [17]. E, E_b and N_0 are the energy of the signal per symbol, the energy of the signal per bit and noise power spectral density, respectively [14]. In the context of this work, the signal refers to the RF carrier waveform. Waveform-level reception simulations, discussed in Section III-C, suggest that γ is in practice determined by the ratio between the energy of the RF carrier and the energy of the noise in the noise BW, each over the time interval T_{BB}.

With OOK, bits 1 and 0 are presented by the presence and absence of the carrier wave [14]. Thus, the carrier is generated only 50% of the time if bits 1 and 0 are equiprobable. Consequently, the local oscillator (LO) and PA can be switched off 50% of the time. OOK can be transmitted and received coherently or noncoherently. However, in this work we mainly discuss noncoherent OOK. It suffers from only minor error performance degradation compared to coherent OOK but avoids carrier synchronization and therefore enables less complex receivers [14]. According to [14], the bit error ratio (BER) with noncoherently received OOK is

$$BER_{OOK} = \frac{1}{2}\Big[1-Q\big(\sqrt{2\cdot\gamma}, b_0\big)\Big] + \frac{1}{2}\exp\Big(-\frac{b_0^2}{2}\Big). \quad (1)$$

Here, $Q(a, b)$ is the Marcum-Q function and $\gamma = A^2/2\sigma^2$ is the SNR in the envelope detector (ED) output. The ED output is ideally Rician [1, Eq. 5] and Rayleigh [1, Eq. 4] distributed when the carrier is received and not received, respectively. A and σ are parameters used in these distributions and they depend on the received signal power and noise power in the noise BW. b_0 is a threshold against which the ED output is compared to decide whether the received bit is 1 or 0. The optimum threshold depends on γ and can be approximated as $b_0 = \sqrt{2+\gamma/2}$ [14], [18]. In the case of OOK, the relationship between the SNR per bit and the SNR is $E_b/N_0 = \gamma/2$ [14].

In this work, we define an active ratio for each modulation for the energy efficiency comparison of Section IV. The active ratio, denoted as $R_{t,mod}$, is the fraction of T_{BB} that the carrier is transmitted per bit. The dominating high-power transmitter blocks, LO and PA, are ideally active for $R_{t,mod}\cdot T_{BB}$ per bit. The lower the active ratio, the lower their energy consumption is per bit. With OOK, if LO and PA are both switched off during the transmission of zeros, the active ratio is $R_{t,OOK} = 0.5$. The energy efficiency comparison shall be made with an equal baseband clock period T_{BB} and equal null-to-null bandwidth, BW_{null}. With OOK, BW_{null} is $2\cdot R_b$ [16], i.e. $2\cdot f_{BB}$.

With BPSK, data is encoded in the phase of the transmitted carrier wave [15], [16]. Coherent BPSK has traditionally been considered more energy efficient than noncoherent OOK and BFSK because it requires lower γ_b for a given BER. For optimum error performance, a coherent BPSK receiver must have a reference waveform accurate in phase and frequency [14], [16] with the received signal. Thus, a coherent BPSK receiver must synchronize with the received carrier. The BER with coherent BPSK [14], [15] is

$$BER_{BPSK} = \frac{1}{2}\cdot \mathrm{erfc}(\sqrt{\gamma}), \quad (2)$$

where $erfc()$ is the complementary error function. In the energy efficiency comparison, we consider the peak output powers as opposed to average powers. For this, the BER is presented here as a function of γ instead of E_b/N_0. With BPSK, the carrier energy per symbol and per bit are equal for which $E_b/N_0 = \gamma$. The carrier is transmitted during the transmission of both ones and zeros for which the active ratio is $R_{t,BPSK} = 1$. The null-to-null BW is $2\cdot R_b$ [16], i.e. $2\cdot f_{BB}$.

With BFSK, the frequency of the transmitted carrier is toggled between two tones that represent bits 1 and 0. BFSK can be transmitted and received either coherently or noncoherently. However, use of coherent BFSK increases transmitter and receiver complexity but achieves only minor improvement in error performance compared to noncoherent BFSK [14]. In this work, we assume use of noncoherent BFSK. Assuming

orthogonal waveforms, the BER with noncoherent BFSK [14], [15], [17] can be written as

$$BER_{BFSK} = \frac{1}{2}\exp\Big(-\frac{\gamma}{2}\Big). \quad (3)$$

In a similar fashion to BPSK, $E_b/N_0 = \gamma$ and the BER is presented here as a function γ as opposed to E_b/N_0. For orthogonality, noncoherent BFSK requires that the two carrier tones f_0 and f_1 are multiples of the bit rate R_b [17]. The preferred frequency separation is hereby $\Delta f = R_b = f_{BB}$ in which case BW_{null} is $3{\cdot}R_b$ [16], i.e. $3{\cdot}f_{BB}$, greater than with OOK or BPSK. A BFSK TX transmits the carrier for T_{BB} per bit and the active ratio is therefore $R_{t,BFSK} = 1$.

III. PPM AND DPPM

M-ary PPM and DPPM possess numerous advantages regarding ULP transmitters. The main advantages are 1) low active ratio and active time per bit, 2) low required SNR per bit for given error performance, 3) low required transmitter complexity, 4) low average power consumption, and 5) that noncoherent reception can be used. The key disadvantages are a lower data rate and longer transmit time compared to OOK, BPSK or BFSK with equal f_{BB}. This can reflect in increased EPB at a receiver. Thus, PPM and DPPM may be best suited for asymmetrical radio links where the receiver side has relaxed energy efficiency requirements compared to the transmitter.

The PPM and DPPM transmit signals resemble an OOK signal in the time domain. The transmitter architecture can therefore be similar to what is used for OOK transmission such as a power oscillator (PO) architecture [2] or a direct-modulation architecture [2]. The modulation can be performed using a low-complexity low-power counter-based digital circuit [1]. Despite the similarity between the signals, PPM and DPPM possess a key advantage over OOK: for optimum error performance, PPM and DPPM reception does not require estimation of the optimum decision threshold based on the SNR. The estimation can be avoided because a receiver can store an array of observed ED output amplitudes and, instead of comparing all amplitudes with an SNR-dependent threshold, it can decide that a given number of slots with the highest amplitudes are the "on" slots and the rest "off" slots. This can be done at the packet level with DPPM using packet-level soft-decision decoding (PL-SDD) [1], and at the symbol level with PPM. A PL-SDD receiver [1, Section VII-A] may practically require an analog-to-digital converter and a digital signal processing (DSP) block which increases receiver complexity compared to, for example, a basic OOK receiver. Calculating the Fourier transforms of OOK-, PPM- and DPPM-encoded RF signals in MathWorks MATLAB suggests that the BW_{null} of both PPM and DPPM are equal to that of OOK, $2{\cdot}f_{BB}$.

A. PPM

With M-ary PPM, B bits are encoded per symbol. The symbol duration is divided into $M = 2^B$ time slots and the data content is defined by the position of a pulse within the slots. As an example, Fig. 1(a) shows 4-PPM symbols. The slots with and without a pulse are called "on" and "off" slots, respectively. The carrier is transmitted for T_{BB} per B bits for which the active ratio is $R_{t,PPM} = 1/B$. The data rate is $R_b = f_{BB} \cdot B/2^B$. In this work, we mainly discuss 16-ary and 64-ary PPM and DPPM. The active ratios with 16-PPM and 64-PPM are 0.25 and 1/6, respectively, and the data rates are $0.25{\cdot}f_{BB}$ and $(6/64){\cdot}f_{BB}$, respectively.

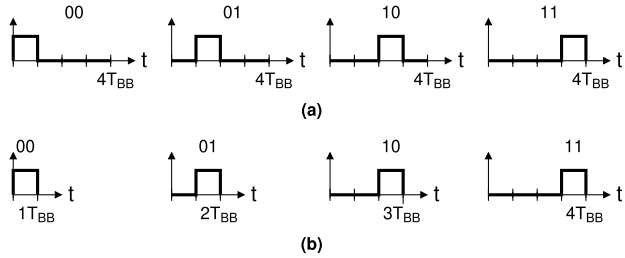

Fig. 1. Baseband waveforms of (a) 4-PPM and (b) 4-DPPM symbols representing 2-bit values 00, 01, 10 and 11.

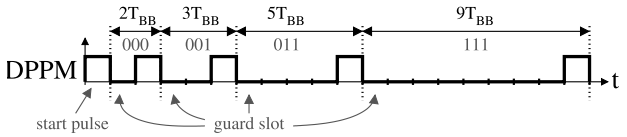

Fig. 2. Example of an 8-DPPM data packet. [1, Fig. 2].

PPM is an orthogonal modulation which, due to the orthogonality, can require very low γ_b for a given error probability [17]. The symbol error ratio (SER) of an orthogonal signal is provided, for instance, in [17] and, acknowledging that $E_b/N_0 = \gamma/B$, the SER with PPM can be written as

$$SER_{PPM} = \sum_{n=1}^{M-1} \frac{(-1)^{n+1}}{n+1}\binom{M-1}{n} \cdot exp\Big(-\frac{n\cdot\gamma}{n+1}\Big). \quad (4)$$

B. DPPM

The time-domain DPPM signal resembles PPM. With DPPM, data is effectively encoded in time intervals between the transmitted pulses. The symbols are PPM symbols where the "off" slots following the "on" slots have been removed [1]. Fig. 1(b) depicts 4-DPPM symbols without guard slots (GSs). Due to shorter symbols, the average data rate is greater compared to PPM with equal B and f_{BB}. When guard slots are added to the symbols, the average data rate is $R_b = 2{\cdot}f_{BB} \cdot B/(2^B + 3)$ [1]. With 16-DPPM and 64-DPPM with guard slots, the average data rates are thus approx. $0.421{\cdot}f_{BB}$ and $0.179{\cdot}f_{BB}$, respectively.

When discussing DPPM in this work, we assume the use of the same packet format that was used previously in [1] with the key features depicted in Fig. 2. The packet begins with a start pulse to which the timing of the pulse of the first symbol is referenced. The start pulse is followed by N_s pulses each of which designates the end of a symbol. N_s is the number of symbols per packet. In the figure, each symbol carries three bits. We use guard slots between the symbols. With the guard slots, two consecutive pulses are always separated by a gap. Each pulse thus produces an individual peak in the ED output at a receiver even when the shortest symbol (000 in Fig. 2) is transmitted. A practical PL-SDD DPPM receiver

implementation [1] can then oversample the ED output and decode the data by calculating the time intervals between the peaks. The uplink measurements of [1] showed that a packet like this can be received with a PL-SDD receiver without carrier or symbol synchronization. Fig. 2 depicts a short packet. However, the transmitter of this paper supports B and N_s up to 6 and 63, respectively.

With DPPM, the active ratio is approximately $1/B$ if the number of symbols per packet is high. In this work, we consider small packets and account for the start pulse. The active ratio is calculated as

$$R_{t,DPPM} = \frac{N_s + 1}{N_s \cdot B}, \tag{5}$$

because, with the start pulse, N_s+1 pulses are transmitted per $N_s \cdot B$ bits. With 48-bit packets, the active ratio is 13/48 and 9/48 with 16-DPPM and 64-DPPM, respectively.

The packet error ratio (PER) with DPPM with noncoherent PL-SDD reception was derived in [1] and is

$$PER_{DPPM} = \int_0^\infty \frac{N_Z r}{\sigma^2} e^{-r^2/2\sigma^2} \left[\int_0^r \frac{r}{\sigma^2} e^{-r^2/2\sigma^2}\, dr \right]^{N_Z-1} \cdot \left\{ 1 - \left[1 - \int_0^r \frac{r}{\sigma^2} e^{-(r^2+A^2)/2\sigma^2} I_0\left(\frac{rA}{\sigma^2}\right) dr \right]^{N_O} \right\} dr. \tag{6}$$

The integration here is performed over variable r. The equation has been derived from Rayleigh and Rician ED output probability density functions that are functions of r and express the probability that the output is r. As mentioned in Section II regarding noncoherent OOK, A and σ are the parameters used in the distributions that depend on the signal and noise powers. $I_0(z)$ is the modified Bessel function of the first kind and zeroth order [14], [18]. N_O is the number of "on" slots in a packet [1], given by

$$N_O = N_s + 1. \tag{7}$$

The maximum number of slots in a packet is given by $L_{p,max}$= 1+N_s·(2^B+1) [1]. N_Z is the maximum number of "off" slots which can be expressed as

$$N_Z = L_{p,max} - N_O = N_s \cdot 2^B. \tag{8}$$

The length of a DPPM packet depends on the data content for which the number of "off" slots can be smaller than N_Z. It can be deduced that, with the discussed packet-mode DPPM scheme, $E_b/N_0 = (N_s+1)\cdot\gamma/N_b$ where $N_b = N_s \cdot B$.

C. Error Performances

The DPPM transmitter of this work transmits 48-bit packets. For this, we shall observe the PERs of OOK, BPSK, BFSK, PPM and DPPM considering a packet size of $N_b = 48$ bits. In communications literature, the energy efficiencies of modulations are often considered by the γ_b they require for BER = 10^{-5}. In this work, we consider an equivalent PER target of $4.8\cdot10^{-4}$ which has been obtained with

$$PER = 1 - (1 - BER)^{N_b}. \tag{9}$$

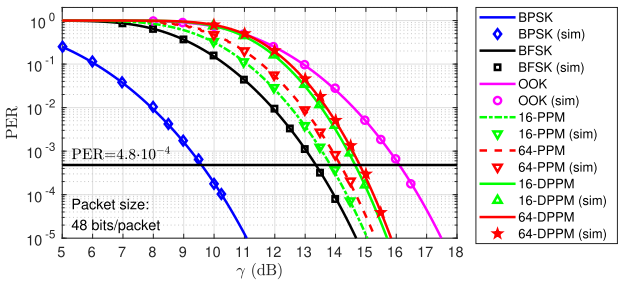

Fig. 3. Theoretical and simulated PERs with the compared modulations against γ. Simulated results are from the waveform-level PER simulations.

Fig. 3 shows the theoretical and simulated PERs against γ as opposed to E_b/N_0. Assuming equal noise BWs, the figure thus effectively visualizes the relationships between the required peak output powers as opposed to required average powers. This is useful for the circuit-related energy efficiency comparison of Section IV. The theoretical PERs of OOK, BPSK and BFSK have been obtained with (1), (2) and (3), respectively, by substituting the results to (9). The theoretical PERs with 16-PPM and 64-PPM have been calculated from the SER, given by (4), as PER = 1–(1–SER)^{N_s}. The theoretical PERs with 16-DPPM and 64-DPPM have been obtained with (6) by numerical integration[1] performed in MATLAB. For the PER calculation with DPPM, N_O and N_Z are obtained with (7) and (8). With 16-DPPM, $B = 4$ bits are encoded per symbol and $N_s = 12$ symbols are required for the 48 bits. For this, $N_O = 13$ and $N_z = 192$. The corresponding values with 64-DPPM are $B = 6$, $N_s = 8$, $N_O = 9$ and $N_Z = 512$.

BPSK, OOK and BFSK require γ of 9.6, 16.1 and 13.4 dB, respectively, for the targeted PER. 16-PPM, 64-PPM, 16-DPPM and 64-DPPM require 13.8, 14.2, 14.6 and 14.8 dB, respectively. OOK and the PPM and DPPM schemes require somewhat greater peak transmit power than BPSK and BFSK. However, the energy efficiency comparison shows that this is well compensated by the lower active ratio – the greater power is transmitted for reduced time per bit.

We have performed waveform-level reception and demodulation simulations in MATLAB. The goal was to verify the validity of the PER calculations and, related to the energy efficiency comparison of Section IV, that noise BW is f_{BB} with all these modulations. Modulated RF signals with the length of a 48-bit packet were generated using all the modulations of Fig. 3. Additive white Gaussian noise (AWGN) was added to the RF signals and reception of the noisy RF signals was simulated using the receivers of Fig. 4. The utilized signal sample rate, carrier frequency and baseband clock period were $f_s = 10$ GHz, $f_c = 434$ MHz and $T_{BB} = 100$ ns, respectively. In the case of BFSK, the first tone was f_c and the second tone $f_{c2} = 444$ MHz. With noncoherent OOK, PPM and DPPM, the RF signal phase was randomized each time the carrier generation started, i.e. when a real duty cycled oscillator would be switched on. With noncoherent BFSK, the phase was randomized each time the transmit tone was changed.

[1](6) is a function of A and σ, not γ. To obtain them from γ, one can choose $A = 1$ and, as $\gamma = A^2/2\sigma^2$, σ is calculated as $\sigma = \sqrt{A^2/2\gamma} = \sqrt{1/2\gamma}$.

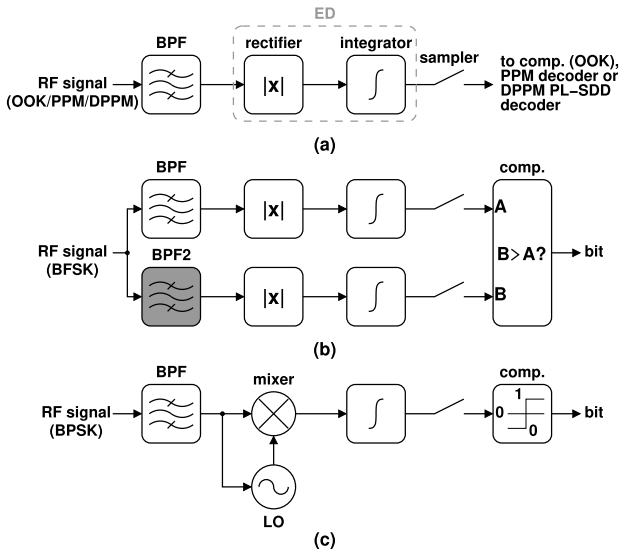

Fig. 4. Block diagrams of the simulated (a) noncoherent OOK/PPM/DPPM receiver, (b) noncoherent BFSK receiver, and (c) coherent BPSK receiver.

The noncoherent OOK, PPM, DPPM and BFSK receivers of Fig. 4(a) and Fig. 4(b) contain bandpass filters BPF and BPF2 that are matched to the transmit tones [15] f_c and f_{c2}, respectively. The BPF and BPF2 finite impulse response (FIR) filter coefficients are sinusoidal waves at f_c and f_{c2}, respectively, with a flat envelope and length T_{BB} (i.e. 1000 samples). The BPFs are followed by an ED [15] that has been implemented here as a full-wave rectifier and an integrator. All receivers, including that of Fig. 4(c), use the same integrator whose integration period is roughly equal to one RF sine cycle, $f_s/f_c \approx 23$ samples. The BPSK receiver front-end consists of the BPF matched to f_c, an LO synchronized to the BPF output signal and a mixer. The samplers in all receivers sample their inputs with a period of T_{BB}.

The sampler outputs were decoded with modulation-dependent methods. OOK output was fed to a comparator. In the simulation, the optimum decision threshold [14] for OOK was estimated separately for each simulated SNR level as $b_0 = \sqrt{2+\gamma_{est}/2}$. Here $\gamma_{est} = A_{est}^2/2\sigma_{est}^2$ where A_{est} and σ_{est} are values of A and σ, respectively, as estimated from the Rayleigh and Rician distributions of the sampled ED output using the *mle()* maximum likelihood estimation function of MATLAB. PPM output was fed to a PPM decoder that, after obtaining 2^B ED output samples during one symbol, decided that the slot with the highest amplitude is the "on" slot and the rest are "off" slots. DPPM output was fed to a PL-SDD decoder that acted in a similar manner at the packet-level: it stored $L_{p,max}$ samples and decided that the slots with the N_s+1 highest amplitudes are the "on" slots and the rest are "off" slots. With BFSK, the two sampled ED outputs were compared with each other to decide the bit. With BPSK, the sampled integrator output was compared with 0 to determine the bit.

The markers in Fig. 3 show the waveform-level reception simulation results. They match well with the theory. The simulated points are plotted against γ, calculated in the simulations as $\gamma = E_{sig}/E_n$ where E_{sig} and E_n are the RF carrier energy per symbol and the noise energy in the noise BW per time interval T_{BB}, respectively. E_{sig} was calculated from the time-domain RF signal as the energy of the carrier wave in a time window the length of T_{BB}. E_n was calculated from the single-sided spectrum of unfiltered AWGN as the energy in the expected noise BW, f_{BB}, per time interval T_{BB}. With each modulation and SNR level, also a second estimate of γ was calculated from the distributions of the sampler outputs. The sampler outputs are Rayleigh and Rician distributed in the noncoherent receivers and Gaussian distributed in the coherent BPSK receiver. A_{est} and σ_{est} were obtained using the *mle()* function and this second estimate of γ was calculated as $\gamma_{est} = A_{est}^2/2\sigma_{est}^2$. The γ estimated this way matched well with E_{sig}/E_n. This shows that the receivers work properly: the SNR at the sampler output is equal to the SNR of the RF signal. As E_n was calculated from the bandwidth f_{BB}, this simulation suggests that the noise BW is f_{BB} with all these modulations. Concerning OOK, BPSK and BFSK, this claim is supported by [19] where, referring to ASK, PSK and FSK, it is said that all digital radio links require receiver noise BW that is equal to the symbol rate. Considering the similarity between OOK, PPM and DPPM signal waveforms, it is somewhat obvious that the pulse-position schemes require similar noise BW as OOK, i.e. f_{BB}, although it is not the symbol rate with them.

IV. Circuit-Related Energy Efficiency Comparison Between OOK, BPSK, BFSK, PPM and DPPM

The energy efficiencies of modulations have traditionally been compared by comparing the γ_b they require for a targeted error performance. The γ_b requirement is highly related to the required average transmit power and, thus, PA power consumption. It largely determines the efficiencies of modulations if the PA dominates the power consumption. However, in ULP applications, the transmitted powers and PA power consumption may be low [2]. Carrier synthesis can consume major power [3] and even dominate the consumption. Thus, it is worthwhile to investigate how the choice of modulation affects the overall energy consumption including blocks other than the PA. ULP transmitters can be implemented without other major blocks besides a carrier synthesizer, a modulator and a PA [2]. The modulator can generally be expected to consume significantly less power than the carrier generation and power amplification. Hereby, we shall analyze how the choice of modulation affects the combined energy consumed per bit by the PA and carrier synthesizer.

This comparison includes OOK, BPSK and BFSK along with M-ary PPM and DPPM. We shall consider how the EPB is affected when, with each modulation, the TX output power is scaled for equal error performance. The modulations are compared here with equal T_{BB} and equal f_{BB}. Due to equal f_{BB}, also the noise bandwidths are equal with all these modulations. For this, Fig. 3 can be directly used to determine the output power scaling. With equal f_{BB}, also the null-to-null BWs are equal with OOK, BPSK, PPM and DPPM, $2{\cdot}f_{BB}$ with each. However, with BFSK, BW_{null} is greater, $3{\cdot}f_{BB}$. [16] For this, we shall consider two BFSK schemes, denoted as BFSK_1 and BFSK_2. BFSK_1 uses the same f_{BB} and T_{BB} as the other modulations but BW_{null} is wider. With

TABLE I
PARAMETERS FOR ENERGY EFFICIENCY COMPARISON CALCULATIONS WITH BPSK AS REFERENCE MODULATION

mod	γ_{req} (dB)	$\Delta\gamma_{req}$ (dB)	$G_{P,mod}$	$R_{t,mod}$
BPSK	9.6	–	1.00	1
OOK	16.1	6.5	4.47	1/2
$BFSK_1$	13.4	3.8	2.40	1
$BFSK_2$	–	–	1.60	1.5
16-PPM	13.8	4.2	2.63	1/4
64-PPM	14.2	4.6	2.88	1/6
16-DPPM	14.6	5.0	3.16	13/48
64-DPPM	14.8	5.2	3.31	9/48

$BFSK_2$, f_{BB} and the frequency separation between the FSK tones are scaled by a factor of 2/3 for equal BW_{null} with the other modulations.

Table I lists the parameters of the modulations required for the energy efficiency calculations, obtained based on the earlier sections. γ_{req} is the γ required for PER $= 4.8{\cdot}10^{-4}$ (see Fig. 3). $\Delta\gamma_{req}$ is the difference in γ_{req} compared to an arbitrarily chosen reference modulation. In this work, BPSK is chosen as the reference. For instance, OOK requires γ of 16.1 dB, BPSK requires 9.6 dB, and $\Delta\gamma_{req}$ with OOK is their difference, 6.5 dB. The power scaling factors, denoted as $G_{P,mod}$, are calculated from $\Delta\gamma_{req}$ as $G_{P,mod} = 10^{(\Delta\gamma_{req})_{dB}/10}$. The last column in the table shows the active ratios. It is to be noted that any energy required for initiating the transmission of a packet is not considered here except in the case of the DPPM schemes. We take into account the start pulse of a DPPM packet in the active ratio and, furthermore, in the PERs of Fig. 3. We consider the error performances when signals are affected by AWGN.

The properties of $BFSK_2$ in Table I are slightly exceptional because of the different f_{BB} and T_{BB} compared to the other modulations. With $BFSK_2$, the baseband clock frequency is $(2/3){\cdot}f_{BB}$ and, consequently, the baseband clock period is $1.5{\cdot}T_{BB}$. For the equations of the next section to apply to $BFSK_2$, we refer its active ratio to the baseband clock period T_{BB} that the other modulations use and denote the active ratio as $R_{t,BFSK2} = 1.5$. The noise BW with $BFSK_2$ is reduced by 1/3 due to the lower f_{BB}. Therefore, for a given γ, it requires 1/3 lower transmit power compared to $BFSK_1$. For this, $G_{P,BFSK2} = (2/3){\cdot}G_{P,BFSK1} \approx 1.60$.

A. Derivation of Equations

To aid in understanding this analysis, Fig. 5 shows examples of power profiles with BPSK, OOK and 64-PPM including powers consumed by an LO and a PA. With LO, we refer to the carrier synthesizer although it could also be a complete PLL or other circuit instead of a bare local oscillator. For simplicity, transmission of only six bits is depicted. In this analysis, we consider how the EPB changes if modulation is changed from the reference modulation to modulation *mod* and output power is scaled for equal error performance. A reference TX uses the reference modulation, in this case BPSK, and its LO and PA consume powers P_{LO} and $P_{PA,ref}$, respectively. The reference BPSK TX transmits six bits in $6{\cdot}T_{BB}$ consuming power $P_{LO}{+}P_{PA,ref}$ for the whole duration. In the figure, P_{LO} and $P_{PA,ref}$ are equal but the equations for this comparison

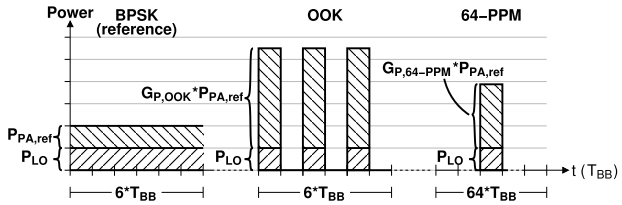

Fig. 5. Power profiles with coherent BPSK, noncoherent OOK and noncoherent 64-PPM with output powers scaled for equal PER.

shall be derived so that they account for various ratios between the LO and PA power consumptions.

In this first scenario, we assume that the other modulations can be performed using the same LO. For this, the LO power consumption is P_{LO} also with OOK and 64-PPM. However, the PA powers of the OOK and 64-PPM TX have been scaled by factors $G_{P,OOK} \approx 4.47$ and $G_{P,64-PPM} \approx 2.88$, respectively, according to Table I. Here, it is assumed that the PA efficiency is not changed for which output power and PA power both scale linearly with $G_{P,mod}$. In a similar fashion to the BPSK TX, the OOK TX transmits the bits in $6{\cdot}T_{BB}$. However, assuming equiprobable bits, the OOK TX transmits the carrier only 50% of the time. Thus, the LO and PA are active for only $3{\cdot}T_{BB}$ per six bits. With the power scaling, the OOK TX consumes power $P_{LO}{+}G_{P,OOK}\cdot P_{PA,ref}$ while the carrier is transmitted. The 64-PPM TX encodes six bits in one symbol and is active for only $1{\cdot}T_{BB}$ per six bits. During that time, it consumes $P_{LO}{+}G_{P,64-PPM}\cdot P_{PA,ref}$. It can be deduced that the EPB is affected by the active ratio. Note that, in Fig. 5, 64-PPM consumes the least energy for the transmission of the six bits.

Based on the above, the EPB can generally be expressed as the product of the power consumption and active time per bit, i.e. as $\text{EPB} = (P_{LO}{+}P_{PA}){\cdot}R_{t,mod}\cdot T_{BB}$. Here, it is assumed that the LO and PA can be switched on and off with negligible overhead time and energy and that they consume zero leakage power. The EPB with the reference modulation is hereby

$$EPB_{ref} = (P_{LO} + P_{PA,ref})\cdot R_{t,ref}\cdot T_{BB}, \tag{10}$$

where $R_{t,ref}$ is the active ratio of the reference modulation. With modulation *mod* that is compared with the reference modulation, the EPB is expressed as

$$EPB_{mod} = (P_{LO} + G_{P,mod}\cdot P_{PA,ref})\cdot R_{t,mod}\cdot T_{BB}. \tag{11}$$

The EPB with modulation *mod* relative to the reference modulation is

$$EPB_{rel,mod} = \frac{EPB_{mod}}{EPB_{ref}}. \tag{12}$$

Substituting (11) and (10) to (12) yields

$$EPB_{rel,mod} = \frac{(P_{LO} + G_{P,mod}\cdot P_{PA,ref})\cdot R_{t,mod}}{(P_{LO} + P_{PA,ref})\cdot R_{t,ref}}. \tag{13}$$

To consider various ratios between the LO and PA powers, we express the relationship between the LO and PA powers of the reference transmitter as

$$P_{PA,ref} = \alpha\cdot P_{LO}. \tag{14}$$

Substituting (14) to (13), we get

$$EPB_{rel,mod} = \frac{(1+\alpha \cdot G_{P,mod}) \cdot R_{t,mod}}{(1+\alpha) \cdot R_{t,ref}}. \quad (15)$$

With (15), the energy efficiencies of modulations can be compared accounting for the combined LO and PA energy consumption. It tells how much the EPB would ideally be after changing modulation from the reference modulation to modulation *mod* with the related output power scaling.

In the derivation of (15) it was assumed that the LO power does not scale at all regardless of output power. However, in some cases, increased output power might also require increased LO power, e.g. if a higher-output-power PA requires greater signal swing at its input which implies greater LO circuitry power consumption. Conversely, decreasing output power could allow for reduced LO power. Thus, let us also consider a scenario where the LO power consumption scales. For simplicity, we consider a scenario where it scales equally with the PA power. In this case, with modulation *mod* that is compared with the reference, P_{LO} is replaced by $G_{P,mod} \cdot P_{LO}$. Performing this modification to (11), we get

$$EPB'_{mod} = G_{P,mod} \cdot (P_{LO} + P_{PA,ref}) \cdot R_{t,mod} \cdot T_{BB}. \quad (16)$$

Furthermore, substituting (10) and (16) to (12), we get

$$EPB'_{rel,mod} = \frac{G_{P,mod} \cdot R_{t,mod}}{R_{t,ref}}. \quad (17)$$

With (17), the energy efficiencies of modulations can be compared in a scenario where the power consumption of the LO scales equally with that of the PA.

B. Energy Efficiency Comparison

Fig. 6 shows the EPBs of OOK, BFSK, 16-PPM, 64-PPM, 16-DPPM and 64-DPPM relative to the EPB of the reference modulation, BPSK, calculated with (15) using values from Table I. The plot is against α, i.e. the ratio between the PA and LO power consumptions of the reference BPSK transmitter. The ratio between the PA and LO powers is not the same with the other modulations because of the output power scaling. Because the output powers are scaled with all modulations for equal error performance with the reference TX, on any vertically drawn line, the modulations can be compared with each other, not just with BPSK.

In Fig. 6 on the right with high α, power consumption is dominated by the PA and the relative energy efficiencies of the modulations are expectedly determined by the γ_b they require for the targeted error performance. However, significant changes can be seen as α falls below 10. The $EPB_{rel,mod}$ of (15) approaches $R_{t,mod}/R_{t,ref}$ as α approaches 0. From $\alpha = 10$ towards $\alpha = 0$, the energy efficiency starts to be more and more impacted by the active ratio. With very low values of α, the energy efficiency of a modulation is mainly determined by the active ratio instead of the SNR per bit required for the targeted error performance. In other words, the less the total TX power consumption is dominated by the PA, the more reasonable it is to use a modulation with a low active ratio. For this, use of M-ary modulations

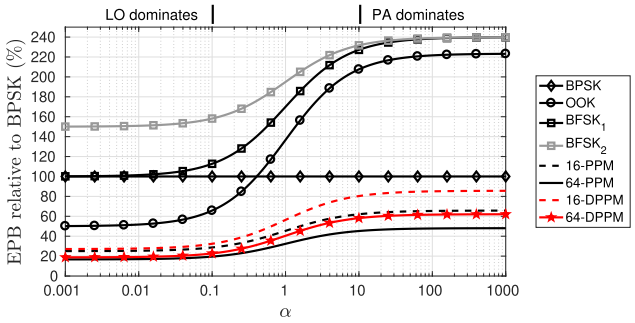

Fig. 6. EPBs relative to coherently detected BPSK without LO power scaling.

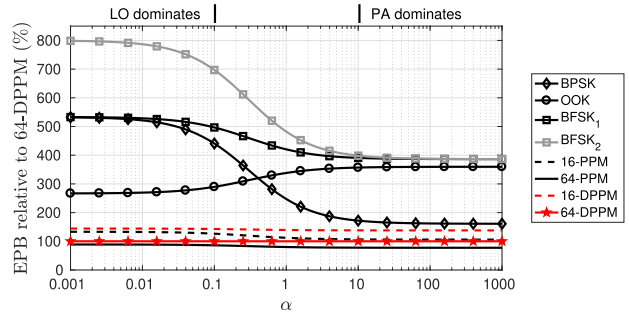

Fig. 7. EPBs relative to 64-DPPM without LO power scaling.

instead of OOK, BPSK and BFSK could be beneficial in ULP applications. In reality, major imbalance between the PA and LO powers may be rarely encountered in ULP transmitters. The regions below $\alpha = 0.1$ and above $\alpha = 10$ may thus represent quite uncommon scenarios. Nonetheless, the impact of the active ratio is visible also at the middle of the plot where the power consumption is not extremely dominated by either of the blocks.

The PPM and DPPM schemes have a low active ratio and require low SNR per bit. Because of these properties, they are expected to achieve good energy efficiency compared to OOK, BPSK and BFSK regardless of which one of the LO and PA blocks dominates. OOK performs well if power consumption is more dominated by the LO and even outperforms BPSK at $\alpha < 0.4$. The figure suggests that the use of OOK and BFSK is not particularly energy efficient when the PA dominates. $BFSK_1$ and $BFSK_2$ are the least energy efficient here at any α. In practice, $BFSK_1$ may be slightly unrealistic because it requires a wider BW than the other modulations. If wider BW was available, it could make sense to use the other modulations with a higher f_{BB} to minimize T_{BB} and the active time per bit. The $BFSK_1$ scheme would then be unable to use wider BW than the other modulations. For this, comparing the modulations with equal BW is reasonable and $BFSK_2$ may provide a more realistic view of BFSK than $BFSK_1$.

For another point of view, Fig. 7 shows the relative EPBs when 64-DPPM is chosen as the reference modulation.[2] If LO dominates, the use of OOK would consume at least 167% more, and the use of BPSK or BFSK at least 341% more energy than 64-DPPM. If the PA dominates, BPSK would consume at least 61% more energy and OOK and BFSK at

[2]The $\Delta\gamma_{req}$ and $G_{P,mod}$ values in Table I need to be recalculated if the reference modulation is changed.

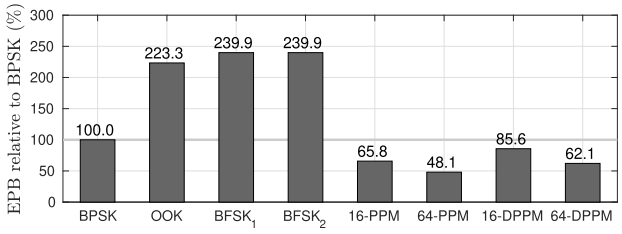

Fig. 8. EPBs relative to BPSK with LO power scaling considered.

least 257% more energy. Looking at the region $0.1 \leq \alpha \leq 10$ in Fig. 7 and comparing it to 64-DPPM, BPSK consumes 72% to 341% more, OOK 190% to 257% more, BFSK_1 291% to 397% more and BFSK_2 298% to 597% more energy.

According to this result, 16-ary and 64-ary PPM and DPPM are considerable options for ULP transmitters. They enable the lowest combined PA and LO energy consumption per bit while still avoiding the carrier synchronization required by BPSK. Particularly, their efficiency is significantly greater compared to OOK and BFSK, the prevailing modulations in published sub-mW transmitters. If higher data rate is desirable, the use of quadrature or 8-ary PPM or DPPM could be considered. With the wide margin here, they could enable good energy efficiency compared to OOK and BFSK while enabling higher data rate compared to the 16-ary and 64-ary variants.

Equation (17) was derived to consider the scenario where the LO power consumption scales equally with the PA power. The result is a constant that depends on the required power scaling factor and active ratios of modulation *mod* and the reference modulation. It is to be noted that (17) is equal to the value that the $EPB_{rel,mod}$ of (15) approaches when α approaches infinity. Thus, in this scenario, the energy efficiency of a modulation is determined by the γ_b it requires for the targeted error performance. Fig. 8 shows the results obtained with (17) using the values of Table I. The PPM and DPPM schemes are the most energy efficient in this scenario too and have a wide margin to OOK and BFSK. The EPBs with OOK and BFSK are more than double compared to BPSK and nearly 4x compared to 64-DPPM. The use of BPSK would consume 61% greater energy compared to 64-DPPM.

V. Figure of Merit for Transmitter Energy Efficiency

Prior ULP transmitter publications have lacked a rational energy efficiency FOM. The EPB has sometimes been considered as the energy-related FOM. It can be expressed as

$$EPB = P_{TX}/R_b, \tag{18}$$

where P_{TX} is the TX power consumption [2]. Some other FOMs are $FOM_{E_{nom}} = \text{EPB}/P_{rad,out}$ [2] and EPB/η [7] where $P_{rad,out}$ and η are the radiated output power and TX power efficiency, respectively. It can be seen that the two latter FOMs are directly proportional to the EPB.

The EPB is not a suitable metric for energy efficiency because it only considers the consumed energy and neglects any output signal metrics such as output power or output energy per bit. Furthermore, it can be relatively easily reduced, i.e. improved, by increasing f_{BB} for higher data rate [1], [2]. The two latter FOMs, being directly proportional to the EPB, also scale with f_{BB}. However, it can be argued that data rate increment by adjusting f_{BB} does not ideally affect energy efficiency. EPB reduction can be achieved easily by clocking the modulator with higher f_{BB} to increase the data rate of e.g. a BFSK TX [8] or an OOK TX [2] from 1 to 10 Mbps. Such a tenfold increment of f_{BB} seemingly improves the three mentioned FOMs ideally tenfold. However, as noise BW is f_{BB}, the tenfold data rate increment also increases the noise BW tenfold and reduces SNR by 10 dB which degrades uplink performance. Considering energy point of view, it reduces T_{BB} and the symbol energy in the TX output signal tenfold. This does not increase energy efficiency. It rather remains approximately constant because the EPB and symbol energy ideally scale by the same amount with T_{BB}. For this, the above FOMs are inadequate metrics of energy efficiency and are unsuitable for comparing transmitters that use different data rates. They also neglect the effect of the used modulation.

In [20], it is discussed that an energy efficiency FOM should take into account the communication range. A comprehensive energy efficiency FOM for transceivers in [20] is

$$Energy\ Efficiency = \frac{P_{out}}{S_{RX}} \cdot \frac{R_b}{P_{TX} + P_{RX}}, \tag{19}$$

where P_{out}, S_{RX} and R_b are output power, receiver sensitivity and data rate, respectively. P_{TX} and P_{RX} are the power consumed by a transmitter and a receiver, respectively. The left side of the equation is link strength $LS = P_{out}/S_{RX}$ [20] and it relates to the achievable uplink range. The right side, $R_b/(P_{TX}+P_{RX})$, is the reciprocal of the energy consumed per bit by both a transmitter and a receiver. The higher the LS is with respect to the energy consumed per bit, the better the energy efficiency is according to (19). This FOM reflects well the energy-related challenge in radio systems: the desirable range should be enabled with the minimum possible energy. The effect of BW and modulation are present in the receiver sensitivity S_{RX}. The greater the BW, the higher S_{RX} is and the more P_{out} is required for sufficient link strength. The less SNR the demodulation of the signal requires, the lower S_{RX} is and the less P_{out} suffices for a given link strength.

By modifying the transceiver-related FOM of (19), a comprehensive energy efficiency FOM can be derived for transmitters that accounts for BW and avoids improper data rate dependency. Let us start by writing the new FOM as a reciprocal of (19) to have the unit as J/bit and dBJ/bit, by removing P_{RX} to consider a transmitter only and, furthermore, by using $\text{EPB} = P_{TX}/R_b$. The FOM becomes

$$FOM = \frac{P_{TX}}{LS \cdot R_b} = \frac{EPB}{LS}. \tag{20}$$

The EPB here refers to the EPB of a transmitter instead of a transceiver. In a transmitter-only system, there is no reference receiver whose sensitivity could be used in determining the link strength. Instead of this, the output signal can be referred to the SNR required by the modulation. This is done by redefining LS as

$$LS' = \gamma_{max}/\gamma_{req}, \tag{21}$$

where γ_{max} and γ_{req} are the maximum SNR achievable with the TX output signal and the SNR required by the modulation

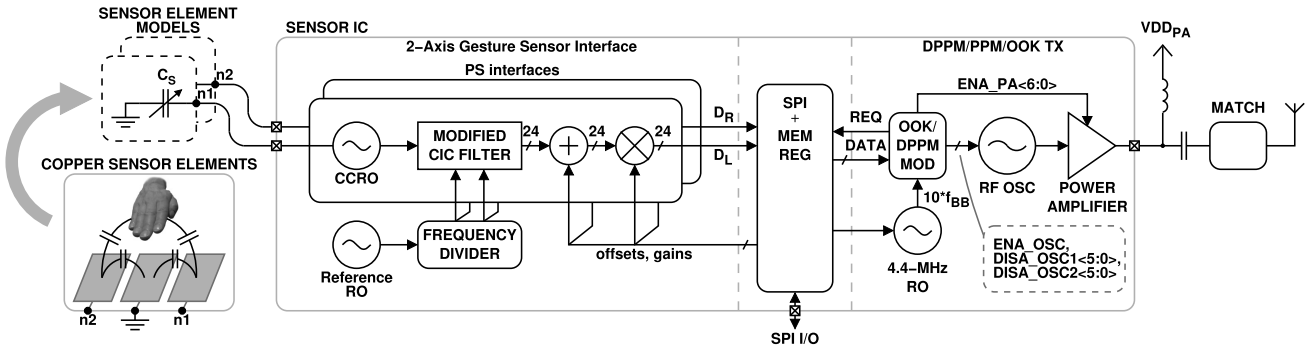

Fig. 9. Block diagram of the system of this work with a capacitive 2-axis gesture sensor interface and a 434-MHz narrowband DPPM/PPM/OOK transmitter.

for targeted error performance, respectively. γ_{max} is the ratio between the output power and noise power in the noise BW, expressed as

$$\gamma_{max} = P_{out}/(k \cdot T \cdot BW), \tag{22}$$

where k, T and BW are the Boltzmann constant, noise temperature in Kelvin and noise BW [17]. We consider the noise at room temperature, i.e. $T = 298$ K. In the case of OOK, BPSK, BFSK, PPM and DPPM, the noise BW is ideally f_{BB} based on the receiver simulations of Section III-C and reference [19]. To only consider the performance achieved by the transmitter circuitry, γ_{max} neglects any power gain that could be achieved, for instance, with antenna gain or caused by constructive interference. Replacing LS in (20) with LS' of (21), we get a short form of the new energy efficiency FOM,

$$FOM = \frac{EPB \cdot \gamma_{req}}{\gamma_{max}}. \tag{23}$$

This can furthermore be written using decibel values as

$$FOM = 10 \cdot \log_{10}\frac{EPB}{1\ \text{J/bit}} + (\gamma_{req})_{dB} - (\gamma_{max})_{dB}. \tag{24}$$

Substituting (18) and (22) to (23) gives an extended form of the FOM,

$$FOM = \frac{P_{TX} \cdot k \cdot T \cdot BW \cdot \gamma_{req}}{R_b \cdot P_{out}}. \tag{25}$$

Notice that (25) is derived from and fully equivalent to (23). In the LS and FOM calculation, P_{out} and γ_{req} are the peak output power and γ requirement discussed in Section III-C, respectively. Alternatively, average TX output power $\overline{P_{out}}$ and $\gamma_{avg,req}$ can be used in the calculations. $\overline{P_{out}}$ is the average output power of a transmitter and $\gamma_{avg,req} = \overline{P_{signal}}/P_n$ the average-signal-power-to-noise-power ratio required by the modulation for the targeted error performance. Both approaches ideally yield the same results.

The unit of this FOM is J/bit or dBJ/bit in decibels and the lower the FOM, the more energy efficient a transmitter can be considered. In a similar fashion to (19), a good FOM is achieved if a transmitter achieves a high link strength relative to the EPB. This FOM is more comprehensive compared to earlier transmitter FOMs as it, justifiably, accounts for the maximum SNR achievable with the generated signal and, through γ_{req}, for the choice of modulation. The less SNR is required for demodulating the signal with a given error performance, the more the output signal may attenuate before the SNR falls below that level. Thus, lower γ_{req} implies higher uplink range. Similarly, a higher output signal SNR increases the range, and the higher the SNR is relative to the EPB, the better the FOM is. The FOM reflects the power efficiency as can be seen in (25) – the greater P_{out} is with respect to P_{TX}, the smaller the FOM is. For the reasons mentioned in the beginning of this section, adjusting the data rate of a given transmitter through f_{BB} does not ideally affect energy efficiency. Correspondingly, this FOM is not impacted much by the choice of f_{BB} as R_b and BW both scale linearly with it. Thus, the keys to good transmitter energy efficiency are the use of power efficient TX circuitry and the use of an energy efficient modulation. In practice, for good power efficiency in low-complexity ULP transmitters, a high-efficiency PA should be used and LO power consumption should be minimized. Note that also increasing f_{BB} can be beneficial if the output power is scaled equally [1] – this maintains the SNR but reduces the energy that e.g. the LO consumes per bit.

It is notable that the FOM can be calculated for various published transmitters. P_{TX}, R_b, P_{out} and modulation are generally reported. The noise BW is known through R_b and modulation. Also the value of γ_{req} depends on the modulation. The FOM can be calculated even if the modulation is other than those that have been discussed in this work such as M-FSK, M-PSK or QAM. The calculation principles also apply to ultra-wide band (UWB) transmitters. Thus, the FOM enables energy efficiency comparison of a wide range of published transmitters regardless of the utilized data rate and modulation.

VI. Circuit Implementation

A. Gesture Sensor Interface

Fig. 9 shows the system block diagram of this work. The main blocks are the gesture sensor interface on the left and the transmitter on the right. The 2-axis gesture sensor interface consists of two proximity sensor (PS) interfaces and the design is based on [21]. Each PS interface contains a capacitance-controlled ring oscillator (CCRO), implemented as a current-starved three-stage ring oscillator (RO). One RO stage is loaded by off-chip sensor plate with capacitance C_s and the two other stages by on-chip capacitors whose capacitance is C_L. For improved phase noise, we use $C_L = 400$ fF here as opposed to 47 fF we used in [21]. When brought near

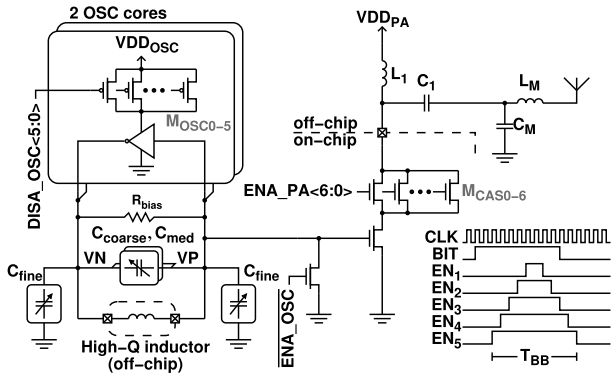

Fig. 10. Schematic of the narrowband transmitter front-end with a Pierce RF oscillator and a PA stage with a matching network.

the sensor plates, the hand of a user increases capacitance C_S which decreases the frequency of the associated CCRO. The output frequencies of the CCROs are converted to digital values using modified decimating 2^{nd} order CIC filters [21]. The filters are clocked using two clock signals generated by dividing the frequency of a reference RO. The operation of the filter is explained in more detail in [21]. As an improvement compared to [21], the filters are followed by on-chip adders and multipliers for correcting the offsets and gains of the sensor data, respectively.

B. Narrowband Transmitter

A schematic of the implemented narrowband transmitter front-end is shown in Fig. 10. It consists of a Pierce RF oscillator and a PA, each with fast start-up. When the carrier is not transmitted, both can be rapidly switched off which enables efficient duty-cycling and, hence, energy efficient DPPM, PPM and OOK modulation.

The Pierce oscillator contains an LC tank comprising tunable on-chip capacitors and an external inductor. The tunable on-chip coarse, medium and fine tuning capacitor designs are identical to those of [1] where they were used by the authors of this work in a power oscillator-based transmitter. The coarse and medium sized tuning capacitors are placed between the nodes VP and VN and have 3-bit and 4-bit controls, respectively. Two 6-bit fine tuning capacitors with independent tuning bits are utilized. For finer frequency tuning step size, one is placed between the node VP and ground and the other between VN and ground. Adding a capacitor between VP (or VN) and ground adjusts the frequency by roughly half the amount compared to adding the same amount of capacitance between VP and VN [22]. An external inductor is utilized because of the relatively low transmission frequency of 434 MHz which requires a high amount of inductance, in the range of a few tens of nH, with the utilized capacitor matrices. To enable sufficient driving strength and fast start-up in slow corners, the oscillator contains two parallel inverters, denoted in Fig. 10 as OSC cores. If a slower start-up is acceptable, the other inverter may be left unutilized which saves power. Furthermore, the oscillator current consumption can be adjusted by disabling part of the header transistors M_{OSC0}–M_{OSC5}.

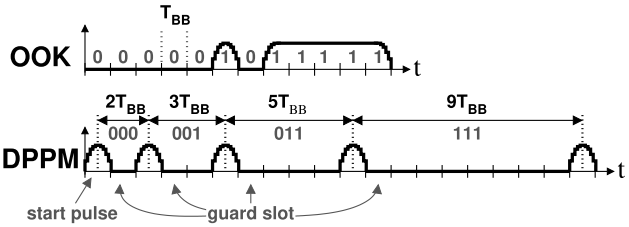

Fig. 11. Examples of OOK and 8-DPPM baseband signals with 10x oversampled pulse shaping.

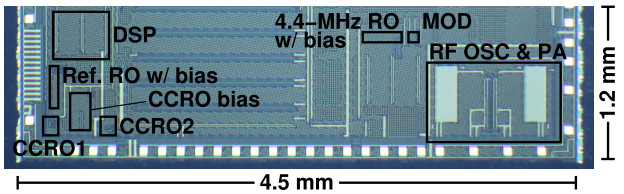

Fig. 12. Micrograph of the circuits, implemented in 0.18 μm CMOS.

To enable pulse shaping, the amplitude of the RF output waveform can be adjusted using the seven cascode transistors M_{CAS0}–M_{CAS6} of the PA. The gate voltage of each cascode transistor, *ENA_PA<6:0>*, can be multiplexed from one of the staggered enable signals EN_1–EN_5, generated by an on-chip modulator and depicted in the bottom right in Fig. 10. The more cascode transistors are enabled, the greater the RF output amplitude is. The longest enable signal, EN_5, is also used to duty cycle the RF oscillator. The output of the PA consists of four off-chip components: RF choke L_1, DC block C_1 and a matching network consisting of L_M and C_M. The PA has been designed to drive a 50Ω load.

The on-chip OOK/DPPM modulator is a modification of [1, Fig. 4] where we have added 1) a state machine that creates the EN_1–EN_5 signals, 2) multiplexing for the *ENA_PA<6:0>* signals, and 3) minor extra logic for handling 1-bit OOK and B-bit DPPM data inputs from the memory register. The modulator enables transmission of OOK, PPM and DPPM data. DPPM can be transmitted with $B = 1$ to $B = 6$ bits encoded per symbol, i.e. using schemes from 2-DPPM to 64-DPPM, with up to 63 symbols per packet. The packet format with a start pulse and guards slots described in Section III-B is used. Fig. 11 shows examples of OOK and 8-DPPM ($B = 3$) baseband signals with pulse shaping. With OOK, the duration of one bit is T_{BB}. With DPPM, the length of each "on" and "off" slot is T_{BB}. The modulator is clocked with a 4.4-MHz current-starved three-stage RO. 10x oversampled pulse shaping [9] is utilized for which the baseband clock frequency of the output signal is $f_{BB} = 4.4$ MHz/10 = 440 kHz. Correspondingly, the baseband clock period is $T_{BB} = 1/f_{BB} \approx 2.27$ μs. By data manipulation,[3] the transmitter supports PPM schemes from 2-PPM to 32-PPM with guard slots. DPPM reception can suffer from insertion and deletion errors [23] which can be avoided by the use of PPM.

[3]DPPM symbols can be converted to PPM symbols by adding the number of removed "off" slots from a previous symbol to the next symbol (see Fig. 1).

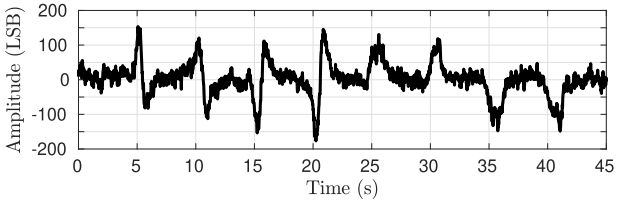

Fig. 13. Differential output of the gesture sensor when gestures are performed with the distance of a palm limited to a minimum of 12 cm.

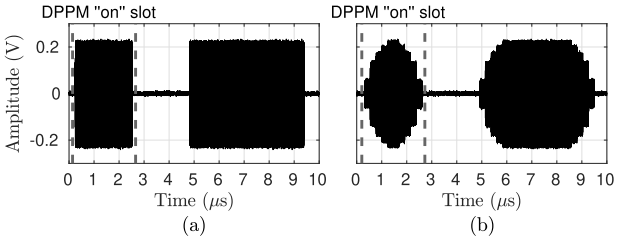

Fig. 14. Output RF waveform of the transmitter (a) without and (b) with pulse shaping showing OOK data 1011. The RF waveform during a DPPM "on" slot is also denoted.

VII. Measurement Results

A micrograph of the implemented gesture sensor and transmitter circuits is shown in Fig. 12. The gesture sensor blocks on the left and transmitter blocks on the right occupy 0.19 and 0.45 mm^2, respectively.

A. Gesture Sensor Measurements

The supply voltage of the CCROs, reference RO and DSP block was set to 0.9 V and the sensor element PCB of [21, Fig. 4] was utilized. The element consists of three 4 cm-by-7 cm copper plates, separated by gaps of 1.5 cm between the longer edges. The left and right CCROs were configured for maximum frequencies, 269 and 219 kHz, to increase the SNR at the cost of power. The frequency of the reference RO was set to 48.4 kHz and the related clock division ratios were set so that the sample rate at the CIC filter output was 47.2 Hz. The power consumptions of the CCROs are 1.43 μW and 1.40 μW. The reference RO and the DSP block consume 13 nW and 0.40 μW, respectively. Thus, the total power consumption of the sensor interface is 3.24 μW.

Fig. 13 shows the differential digital output of the sensor interface (i.e. left side PS output subtracted from the right side PS output, D_R–D_L) during hand sweep and push gestures. To limit the minimum distance between the palm and the sensor plates, two plastic rails were placed above the plates codirectionally with the plane of the sensor plates. The performed eight gestures were two sweeps from left to right, two sweeps from right to left, two pushes over the left plate, and two pushes over the right plate. The gestures are distinguishable in the data, obtained with the distance of the palm limited to 12 cm. The RMS noise of the differential output is 15.9 LSBs and the signal amplitudes are greater than 80 LSBs.

B. Transmitter Measurements

The supply voltage of the RF oscillator and PA was set to 0.9 V. The 4.4-MHz RO and the modulator were supplied with 1.2 V. In continuous-wave transmission with the frequency tuned to 434 MHz, the RF oscillator and PA consume 316 μW and 1 337 μW, respectively, and the output power is -2.1 dBm. Thus, the peak PA drain efficiency and peak total efficiency of the TX front-end are 46% and 37%, respectively. The leakage powers of the LO and PA are 0.1 and 0.9 nW, respectively. A 27–nH Coilcraft 0805CS series inductor is used in the LC tank. The typical Q is approx. 70 at 434 MHz. The carrier tuning range is from 484.6 to 426.5 MHz and the frequency resolution is better than 41 kHz throughout this range. The frequency of the 4.4-MHz RO was tuned to 4.398 MHz which results in a baseband clock frequency f_{BB} = 439.8 kHz. The 4.4-MHz RO consumes 564 nW of power.

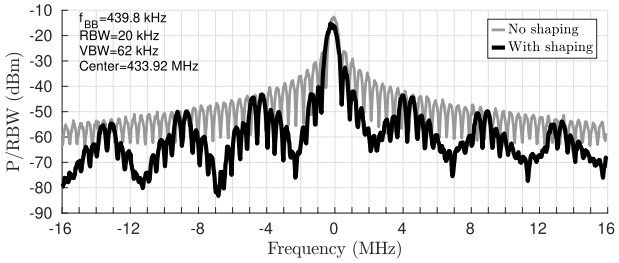

Fig. 15. Output spectrum of the transmitter with and without pulse shaping when transmit data is a repeating 1010 OOK data pattern.

TABLE II
Continuous-Mode TX Results With Pulse Shaping

Modulation	OOK	16-DPPM	64-DPPM
Bits/symbol, B	1	4	6
Power Consumption (μW)	736	140	41.1
Average Data Rate (kbps)	440	185 †	78.8 †
Average Output Power (dBm)	-6.2	-14.3	-19.8
TX Efficiency	32.6%	26.5%	25.5%
EPB (nJ/bit)	1.67	0.76	0.52

† With DPPM with GS, data rate is $2{\cdot}f_{BB} \cdot B/(2^B + 3)$. [1, Eq. 3]

Fig. 14 shows examples of the TX output waveform with the OOK data pattern 1011 with and without pulse shaping. Also the waveform during a DPPM/PPM "on" slot is denoted. Fig. 15 shows the effect of the shaping in the frequency domain with the TX continuously transmitting a repeating OOK data pattern 1010 which produces the greatest OBW. This RF waveform is also equivalent to a DPPM data stream using zero-only symbols with guard slots. The OBW was measured using a Keysight N9041B UXA signal analyzer with a span of 32 MHz to include the major sidebands. With pulse shaping and f_{BB} = 439.8 kHz, the OBW is 1.65 MHz and the ETSI OBW requirement of 1.75 MHz (from 433.04 to 434.79 MHz) [24] is met.

Table II shows the measured power consumption, output power, TX efficiency and the EPB during continuous-mode transmission of randomized OOK, 16-DPPM and 64-DPPM data with pulse shaping enabled. With OOK, 50% of the bits were ones to obtain average power consumption and output power. The power consumption includes the consumption of the RF oscillator, PA, 4.4-MHz RO, modulator and the additional digital logic that control the Pierce RF oscillator header transistors and the PA cascode transistors. With OOK, an EPB of 1.67 nJ/bit and a TX efficiency of 32.6% are

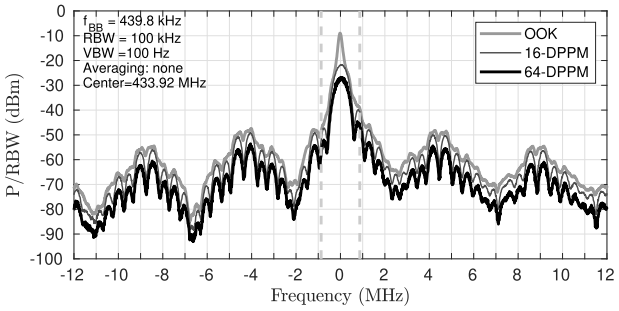

Fig. 16. Spectra of the output signal with continuously transmitted randomized data. Pulse shaping is enabled.

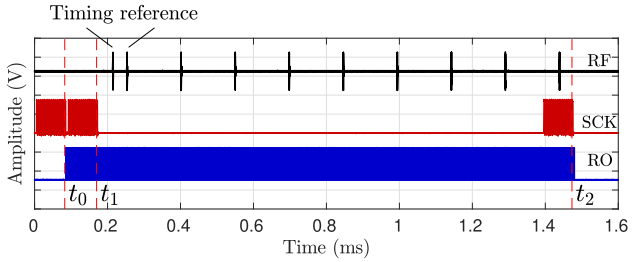

Fig. 17. RF output, SPI clock line (SCK) and 4.4-MHz RO output when a 48-bit DPPM data packet is transmitted. The waveforms are not in the same vertical scale.

achieved. With 64-DPPM, the EPB and TX efficiency are 0.52 nJ/bit and 25.5%, respectively, i.e. the EPB is 69% lower. Fig. 16 shows the output signal spectra corresponding to the transmit modes of Table II. With DPPM, the average output power is lower than with OOK. However, this does not imply a lower uplink range. If a given OOK transmitter is converted to transmit 64-DPPM data with equal f_{BB}, the EPB and power consumption ideally decrease by 67% and 94%, respectively, but error performance is not expected to decrease because 64-DPPM requires lower γ [1]. This assumes a non-shaped pulse envelope. In this work, the shaping has an impact but the uplink ranges with both modulations are expected to be very similar. 64-DPPM thus achieves the LS with lower EPB.

C. TX Results / Packet-Mode 64-DPPM Data Transmission

Packet-mode transmission was tested using 48-bit data packets consisting of a timing reference symbol and eight 64-DPPM symbols. With 48 bits, the two raw 24-bit PS output samples can be transmitted. As the sensor accuracy is lower, truncated, for example, 16-bit values could be transmitted with other bits used for error detection or correction. An FPGA was used to control the TX through the SPI. Fig. 17 shows the SPI clock line (SCK), 4.4-MHz RO output and RF output during the transmission of a single packet. The two first SPI bursts start up the 4.4-MHz RO and trigger the data transmission at t_0 and t_1, respectively. To save power until the next packet is transmitted, the third SPI burst stops the 4.4-MHz RO at t_2. With the start pulse and timing reference, a packet consists of a total of 10 pulses. All eight data symbols here consist of data 111111_2, i.e. the symbol with the longest duration, and the figure thus depicts the longest packet.

With pulse shaping enabled and 47.2 packets transmitted per second, the TX consumes 1.56 μW of power. The RF oscillator, PA, digital circuitry (modulator and other logic circuits that control the LO and PA) and baseband RO consume 346 nW, 1.05 μW, 46 nW and 116 nW, respectively. As the data rate is 47.2·48 bps = 2265.6 bps, the EPB is 0.69 nJ/bit. This EPB is higher than in continuous-mode transmission mainly because additional energy is used to generate the start pulse and the timing reference symbol.

D. FOM Evaluation and Comparison

The DPPM PER in (6) assumes packet-mode transmission and use of PL-SDD at the receiver. For this, we evaluate the FOM considering the performance in the previous packet-mode measurement using 64-DPPM and with the EPB of 0.69 nJ/bit. The FOM is evaluated with (24). Here, γ_{req} must be recalculated because the timing reference symbol adds one "on" slot and 16 "off" slots to the packet compared to the 64-DPPM packet format discussed in Sections III-B and III-C. This increases N_O and N_z to 10 and 528, respectively, and affects the PER. We recalculated the PER given by (6) and γ required for PER = $4.8{\cdot}10^{-4}$. The effect of the greater N_O and N_Z is almost negligible and γ_{req} is 14.8 dB also with the additional symbol. Furthermore, we evaluated the effect of the pulse shaping on the PER by performing waveform-level PER simulations according to Section III-C using the pulse envelope of Fig. 14(b) in the emulated DPPM RF signal. The FIR coefficients of the BPF of the receiver in Fig. 4(a) were changed to match with the signal envelope. With this proper filtering, the shaping did not impact the error performance. γ at the sampled ED output was still directly determined by E_{sig}/E_n where E_{sig} is now the energy of an envelope-shaped symbol waveform and E_n the energy of the noise in bandwidth f_{BB} over the time interval T_{BB}. This implies that the noise BW is f_{BB} also with the shaping.

Based on the above and the earlier sections, γ_{max} is $\gamma_{max} = E_{out}/E_n = (P_{out} \cdot T_{BB})/(P_n \cdot T_{BB}) = P_{out}/P_n$. However, because shaping is used and P_{out} is not constant, we calculate this as $\gamma_{max} = P_{out,eff}/P_n$, where $P_{out,eff}$ is the effective output power during an "on" slot. When the 1010 pulse train was transmitted with pulse shaping enabled, the measured output power was −7.5 dBm. Because a pulse was included in every other slot, $P_{out,eff}$ is twice this much, $P_{out,eff} = -4.5$ dBm. The noise power in BW of 440 kHz is $P_n = k \cdot T \cdot BW \approx -117.4$ dBm. Hereby, we get $\gamma_{max} = (P_{out,eff})_{dB} - (P_n)_{dB} = 112.9$ dB. With EPB = 0.69 nJ/bit, $\gamma_{req} = 14.8$ dB and $\gamma_{max} = 112.9$ dB, the energy efficiency FOM as given by (24) is −189.7 dBJ/bit.

Table III shows a comparison between this work, denoted as T. W., and other ULP transmitters including three Bluetooth Low Energy (BLE) TXs. The table lists the properties in continuous-mode data transmission that suffice for calculating the FOM using (25).[4] $\overline{P_{TX}}$ and $\overline{P_{out}}$ are the average power consumption and average transmit power. As was discussed in Section V, to calculate the FOM using

[4]We evaluated the FOM of our TX using (24) as opposed to (25) but the equations are equivalent and the FOM results are comparable.

TABLE III
ENERGY EFFICIENCY COMPARISON OF ULP NARROWBAND TXS

	Modulation	$\overline{P_{TX}}$[1] [μW]	$\overline{P_{out}}$[1] [dBm]	R_b[1] [kbps]	EPB[1] [pJ/bit]	FOM[2] [dBJ/bit]
T. W.	64-DPPM[3]	41	-19.8	78.8	522	-189.7[4]
[13]	BPSK	67	-17.5	1000	67	-188.5
[25]	GFSK/BLE	1550	-3.3	1000	1550	-186.2
		490	-19	1000	486	-175.5
[9]	BPSK	530	-11	1000	530	-186.0
	OOK[3]	440	-12.5	1000	440	-181.8
[26]	GFSK/BLE	4000	0	1000	4000	-185.4
[5]	BPSK	330	-15	20000	16.5	-184.1
[3]	BFSK	90	-17	200	450	-183.9
[6]	OOK[3]	2600	≈ -3.2	40000	64.5	-183.4
[12]	BFSK	700	-10	5000	140	-182.0
[10]	OOK[3]	518	-12.7	10000	52	-180.9
[8]	BFSK	170	-20	1000	170	-178.2
		180	-20	10000	18	-177.9
[7]	OOK[3]	600	-17	20000	30	-175.9
[1]	64-DPPM[3]	10.4	-40[5]	895.5	11.6	-175.6[4]
[11]	OOK[3]	248	-24	1000	248	-172.8
[27]	GFSK/BLE	606	-23.4[5]	1000	606	-170.2
[4]	OOK[3]	191	-29[5]	5000	38	-168.9
	BFSK	374	-26[5]	5000	75	-168.7

1) Average during continuous transmission of modulated data.
2) FOM as discussed in Section V. Takes into account P_{TX}, P_{out}, power efficiency, EPB, R_b and SNR required by modulation.
3) Average duty cycle is 50% with OOK and 3.0% with 64-DPPM with guard slot.
4) FOM of DPPM TX evaluated based on performance in packet-mode transmission, not continuous-mode.
5) PO-based TX. Output power as limited by fixed coil-antenna.
6) Carrier frequency is 920 MHz in [12], 2.4 to 2.48 Ghz in [25], [9], [26], [7], [27] and [4], and otherwise 400 to 480 MHz.

average output power, γ_{req} in (25) must be replaced with the average-signal-power-to-noise-power ratio required by the modulation, $\gamma_{avg,req}$. With BPSK, OOK and BFSK, $\gamma_{avg,req}$ is 9.6, 13.1 and 13.4 dB, respectively, for BER $= 10^{-5}$ and PER $= 4.8{\cdot}10^{-4}$. The noise BW with these modulations is R_b. BLE transmitters use a modulation index h between 0.45 and 0.55 and a bandwidth-bit period product BT of 0.5 [28]. Assuming noncoherent GFSK reception and the use of $h = 0.5$, bit error probability is the same as with BFSK [29], and $\gamma_{avg,req}$ is 13.4 dB. With GFSK, the noise BW is obtained as $BW = \sqrt{\pi/(4 \cdot log_{10}(2))} \cdot BT \cdot R_b$. [30].

The transmitters included in the table are sorted by FOM from best to worst. The TX of this work achieves the best FOM. Also the BPSK and high-output-power BLE TXs achieve good FOMs. The FOM differences are mainly explained by differences in the TX power efficiencies and energy efficiencies of the modulations. Power efficiency degradation degrades the FOM linearly and e.g. tenfold reduction of efficiency degrades the FOM by 10 dB. The choice of modulation has an effect up to several decibels here. It can be seen that the EPB and power consumption do not correlate much with the energy efficiency FOM. It can be pointed out that any of the OOK, BPSK, BFSK or GFSK TXs could be duty cycled for lower average power consumption. However, that would ideally not impact the TX energy efficiency nor the FOM. As per (23) and because $\gamma_{max} = E_{out}/E_n$, the FOM ultimately only considers symbol energy in the output signal, the corresponding noise energy, how much energy is consumed per bit in the transmit process and γ required by the modulation. Duty cycling, i.e. adding gaps between the symbols or packets, would ideally not impact these parameters.

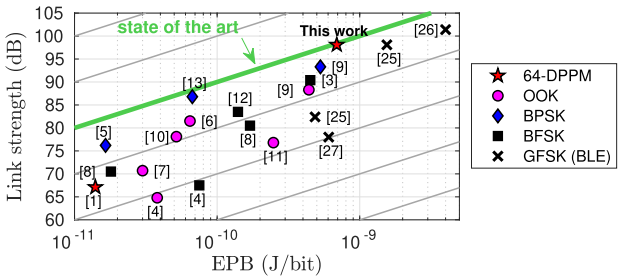

Fig. 18. Link strengths of the works included in Table III versus EPBs.

Regarding energy efficiency, the main challenge is in achieving a given link strength with a low EPB. The link strengths of the transmitters of Table III can be calculated with (21) and (22), or simply as $LS = 10{\cdot}\log_{10}(\text{EPB}/(1\text{ J/bit}))–(\text{FOM})_{dB}$ as per (24). They are plotted in Fig. 18 against the EPBs. The LS in this work is $(\gamma_{max})_{dB}–(\gamma_{req})_{dB} = (112.9\text{-}14.8)$ dB $= 98.1$ dB. A general trend is visible: a low EPB also implies lower link strength and uplink range. The presented new FOM expresses how high the LS is relative to the EPB. The closer the FOM is to -190 dBJ/bit, the closer the TX is to the diagonal line that denotes the current state of the art in energy efficiency.

The 64-DPPM transmitter we presented in [1], located on the bottom left in Fig. 18 and also operating at a carrier of 434 MHz, achieved a 30-meter line-of-sight (LOS) uplink in measurements without exploiting directional antennas. In this work, the link strength is roughly 31 dB greater compared to [1] which enables greater range. From free-space loss [31], it can be calculated that 31 dB equals to an uplink range increment by a factor of $10^{31/20} \approx 35.5$. With just 0.69 nJ consumed per bit, this TX thus enables an LOS uplink range up to 1 kilometer.

VIII. CONCLUSION

The energy efficiencies of modulations were compared accounting for combined power consumed by PA and LO. According to the results, OOK, BPSK and BFSK may consume tens to hundreds of percents more energy per bit than M-ary PPM and DPPM depending on the scenario. Furthermore, a comprehensive transmitter energy efficiency FOM was derived that can be used for comparing various types of transmitters regardless of data rate and modulation. The presented circuits consisted of a sub-100μW transmitter and a 3.2-μW gesture sensor interface. The transmitter achieves a remarkably good FOM due to good power efficiency and the use of an energy efficient modulation. The estimated uplink range of 1 km is worthy of note considering the low power consumption.

ACKNOWLEDGMENT

The authors would like to thank M.Sc. Jarno Salomaa, D.Sc. Tuomas Haapala, and M.Sc. Mohammad Mehdi Moayer for help with the chip design and tape out, and M.Sc. Doru Irimescu for designing the measurement PCB.

REFERENCES

[1] M. Pulkkinen, T. Haapala, J. Salomaa, and K. A. I. Halonen, "Low-power wireless transceiver with 67-nW differential pulse-position modulation transmitter," *IEEE Trans. Circuits Syst. I, Reg. Papers*, vol. 67, no. 12, pp. 5468–5481, Dec. 2020.

[2] D.-G. Lee, L. G. Salem, and P. P. Mercier, "Narrowband transmitters: Ultralow-power design," *IEEE Microw. Mag.*, vol. 16, no. 3, pp. 130–142, Apr. 2015.

[3] J. Pandey and B. P. Otis, "A sub-100 μW MICS/ISM band transmitter based on injection-locking and frequency multiplication," *IEEE J. Solid-State Circuits*, vol. 46, no. 5, pp. 1049–1058, May 2011.

[4] P. P. Mercier, S. Bandyopadhyay, A. C. Lysaght, K. M. Stankovic, and A. P. Chandrakasan, "A sub-nW 2.4 GHz transmitter for low data-rate sensing applications," *IEEE J. Solid-State Circuits*, vol. 49, no. 7, pp. 1463–1474, Jul. 2014.

[5] Y.-L. Tsai, C.-Y. Lin, B.-C. Wang, and T.-H. Lin, "A 330-μW 400-MHz BPSK transmitter in 0.18-μm CMOS for biomedical applications," *IEEE Trans. Circuits Syst. II, Exp. Briefs*, vol. 63, no. 5, pp. 448–452, May 2016.

[6] J. Ryu, M. Kim, J. Lee, B.-S. Kim, M.-Q. Lee, and S. Nam, "Low power OOK transmitter for wireless capsule endoscope," in *IEEE MTT-S Int. Microw. Symp. Dig.*, Jun. 2007, pp. 855–858.

[7] S.-Y. Lee, P.-H. Cheng, C.-F. Tsou, C.-C. Lin, and G.-S. Shieh, "A 2.4 GHz ISM band OOK transceiver with high energy efficiency for biomedical implantable applications," *IEEE Trans. Biomed. Circuits Syst.*, vol. 14, no. 1, pp. 113–124, Feb. 2020.

[8] M. A. A. Ibrahim and M. Onabajo, "A low-power BFSK transmitter architecture for biomedical applications," *IEEE Trans. Circuits Syst. I, Reg. Papers*, vol. 67, no. 5, pp. 1527–1540, May 2020.

[9] A. Paidimarri, P. M. Nadeau, P. P. Mercier, and A. P. Chandrakasan, "A 2.4 GHz multi-channel FBAR-based transmitter with an integrated pulse-shaping power amplifier," *IEEE J. Solid-State Circuits*, vol. 48, no. 4, pp. 1042–1054, Apr. 2013.

[10] M. K. Raja and Y. P. Xu, "A 52 pJ/bit OOK transmitter with adaptable data rate," in *Proc. IEEE Asian Solid-State Circuits Conf.*, Nov. 2008, pp. 341–344.

[11] H.-C. Cheng, Y.-T. Chen, P.-H. Chen, and Y.-T. Liao, "An optically-powered 432 MHz wireless tag for batteryless Internet-of-Things applications," *IEEE Trans. Circuits Syst. I, Reg. Papers*, vol. 66, no. 9, pp. 3288–3295, Sep. 2019.

[12] J. Bae, L. Yan, and H.-J. Yoo, "A low energy injection-locked FSK transceiver with frequency-to-amplitude conversion for body sensor applications," *IEEE J. Solid-State Circuits*, vol. 46, no. 4, pp. 928–937, Apr. 2011.

[13] S. Mondal and D. A. Hall, "A 67-μW ultra-low power PVT-robust MedRadio transmitter," in *Proc. IEEE Radio Freq. Integr. Circuits Symp. (RFIC)*, Los Angeles, CA, USA, Aug. 2020, pp. 327–330.

[14] M. Schwartz, W. R. Bennett, and S. Stein, *Communication Systems and Techniques*. New York, NY, USA: McGraw-Hill, 1966.

[15] S. Haykin, *Communication Systems*, 4th ed. Hoboken, NJ, USA: Wiley, 2001.

[16] F. Xiong, *Digital Modulation Techniques*, 2nd ed. Norwood, MA, USA: Artech House, 2006.

[17] J. G. Proakis and M. Salehi, *Digital Communications*, 5th ed. New York, NY, USA: McGraw-Hill, 2008.

[18] Q. Tang, S. K. S. Gupta, and L. Schwiebert, "BER performance analysis of an on-off keying based minimum energy coding for energy constrained wireless sensor applications," in *Proc. IEEE Int. Conf. Commun. (ICC)*, vol. 4, May 2005, pp. 2734–2738.

[19] A. G. Phadke, *Handbook of Electrical Engineering Calculations*. Boca Raton, FL, USA: CRC Press, 1999.

[20] R. Taherkhani and S. Nihtianov, "An energy efficiency figure of merit for radio transceivers," in *Proc. IEEE Radio Antenna Days Indian Ocean (RADIO)*, Sep. 2019, pp. 1–2.

[21] M. Pulkkinen, J. Salomaa, M. M. Moayer, T. Haapala, and K. Halonen, "462-nW 2-axis gesture sensor interface based on capacitively controlled ring oscillators," in *Proc. IEEE Int. Symp. Circuits Syst.*, May 2017, pp. 1–4.

[22] N. M. Pletcher and J. M. Rabaey, "A 100 μW, 1.9 GHz oscillator with fully digital frequency tuning," in *Proc. IEEE Eur. Solid-State Circuits Conf.*, Sep. 2005, pp. 387–390.

[23] U. Sethakaset and T. Gulliver, "Soft-decision decoding for differential pulse-position modulation (DPPM) over optical wireless communications," in *Proc. IEEE Veh. Technol. Conf.*, Montreal, QC, Canada, Sep. 2006, pp. 1–5.

[24] *Electromagnetic Compatibility and Radio Spectrum Matters (ERM); Short Range Devices (SRD); Radio Equipment to be Used in the 25 MHz to 1000 MHz Frequency Range With Power Levels Ranging up to 500 mW; Part 1: Technical Characteristics and Test Methods*, Standard EN 300 220-1, Version 2.4.1, European Standard, European Telecommunications Standards Institute, Jan. 2012.

[25] X. Chen et al., "Analysis and design of an ultra-low-power Bluetooth Low Energy transmitter with ring oscillator-based ADPLL and 4× frequency edge combiner," *IEEE J. Solid-State Circuits*, vol. 54, no. 5, pp. 1339–1350, May 2019.

[26] S. Yang, J. Yin, H. Yi, W.-H. Yu, P.-I. Mak, and R. P. Martins, "A 0.2-V energy-harvesting BLE transmitter with a micropower manager achieving 25% system efficiency at 0-dBm output and 5.2-nW sleep power in 28-nm CMOS," *IEEE J. Solid-State Circuits*, vol. 54, no. 5, pp. 1351–1362, May 2019.

[27] Y. Shi, X. Chen, H.-S. Kim, D. Blaauw, and D. Wentzloff, "A 606μW mm-scale Bluetooth Low Energy transmitter using co-designed $3.5\times3.5\text{mm}^2$ loop antenna and transformer-boost power oscillator," in *IEEE Int. Solid-State Circuits Conf. (ISSCC) Dig. Tech. Papers*, Feb. 2019, pp. 442–444.

[28] *Bluetooth Core Specification*, Rev. 5.2, Bluetooth SIG, Kirkland, WA, USA, Dec. 2019.

[29] J. R. Luque, M. J. Morón, and E. Casilari, "Analytical and empirical evaluation of the impact of Gaussian noise on the modulations employed by Bluetooth enhanced data rates," *EURASIP J. Wireless Commun. Netw.*, vol. 94, pp. 113–124, Mar. 2012.

[30] D. McMahill, *Automated Calibration of Modulated Frequency Synthesizers*. Boston, MA, USA: Kluwer Academic, 2002.

[31] *IEEE Standard for Definitions of Terms for Antennas*, IEEE Standard 145-2013, Mar. 2014.

Mika Pulkkinen (Member, IEEE) received the B.Sc. degree in electrical engineering from Aalto University School of Electrical Engineering, Espoo, Finland, and the M.Sc. degree in micro- and nanotechnology from Aalto University School of Electrical Engineering, in 2014. He is currently working to finalize his D.Sc. thesis with the Electronic Circuit Design Group, Department of Electronics and Nanotechnology, Aalto University. He is also with CoreHW Oy. His research interests include design of low-power digital, analog and RF circuits.

Kari Halonen (Member, IEEE) received the M.Sc. degree in electrical engineering from the Helsinki University of Technology, Finland, in 1982, and the Ph.D. degree in electrical engineering from the Katholieke Universiteit Leuven, Belgium, in 1987. He became the Head of the Electronic Circuit Design Laboratory in 1998 and he was appointed as the Head of the Department of Micro and Nano sciences, Aalto University, from 2007 to 2013. Since 1988, he has been with the Electronic Circuit Design Laboratory, Helsinki University of Technology (since 2011 Aalto University), Espoo, Finland. Since 1993, he has been an Associate Professor with the Faculty of Electrical Engineering and Telecommunications, where he has also been a Full Professor since 1997. He specializes in CMOS and BiCMOS analog and RF integrated circuits, particularly for telecommunication and sensor applications. He has authored or coauthored over 450 international and national conference and journal publications on analog and RF integrated circuits. He has served as a TPC member for ESSCIRC and ISSCC. He was awarded the Beatrice Winner Award in the ISSCC Conference 2002. He was the Technical Program Committee Chairman of the European Solid-State Circuits Conference 2000 and 2011. He was an Associate Editor of IEEE JOURNAL OF SOLID-STATE CIRCUITS and IEEE TRANSACTIONS ON CIRCUITS AND SYSTEMS—I: REGULAR PAPERS and a Guest Editor of IEEE JOURNAL OF SOLID-STATE CIRCUITS.